JOC The Journal of Organic Chemistry

Article

pubs.acs.org/joc

Regioselectivity in the Cu(I)-Catalyzed [4 + 2]-Cycloaddition of 2-Nitrosopyridine with Unsymmetrical Dienes

Anh T. Tran,[†] Peng Liu,[‡] K. N. Houk,[‡] and Kenneth M. Nicholas*[,†]

[†]Departments of Chemistry and Biochemistry, University of Oklahoma, Norman, Oklahoma 73019, United States

[‡]University of California at Los Angeles, Los Angeles, California 90095, United States

Supporting Information

ABSTRACT: The thermal (uncatalyzed) and Cu(I)-catalyzed reactions of 2-nitrosopyridine (PyrNO) with the dienes 1,3-pentadiene, *E,E*-2,4-hexadienol, and 1-phenylbutadiene are investigated experimentally and computationally. The uncatalyzed reactions of the first two dienes occur with low regioselectivity, while the latter proceeds with complete *proximal* selectivity. Using the M06/6-311+G(d,p)−SDD method, various concerted transition states for the reactions of 2-nitrosopyridine with (*E*)-1,3-pentadiene and 1-phenylbutadiene were computed. In quantitative agreement with the experimental findings, (a) no energy difference (0.0 kcal/mol) is found between the most stable transition states, *endo-prox-anti* and *endo-dist-anti,* in the pentadiene/PyrNO reaction, leading to nearly equal amounts of *prox* and *dist* cycloadducts, and (b) the *proximal* transition state is strongly favored (by 3.7 kcal/mol) over the *distal* for the highly selective phenylbutadiene/PyrNO reaction. The regioselectivity of the pentadiene/PyrNO reaction is improved markedly (90:10 *dist*/*prox*) when catalyzed by $Cu(CH_3CN)_4^+$; $(diimine)_2Cu^+$ catalysts increase selectivity for the *proximal* product (55−65%). Modest effects of the catalyst nature on regioselectivity are observed in the sorbyl alcohol and 1-phenylbutadiene reactions. The relative affinity of an equilibrating set of $(diimine)_2Cu^+$ complexes for the *prox* and *dist* cycloadducts, assessed by ESI-MS, is marginally correlated with the *prox*/*dist* product regioselectivity produced by the corresponding catalysts. Transition states in the $Cu(CH_3CN)_4^+$- and $Cu(diimine)_2^+$-catalyzed reactions are located that account for the observed regioselectivities. Coordination effects on the regioselectivity are derived from FMO orbital interactions and the extent of electron transfer between the Cu center and the coordinated nitroso and diene units.

1. INTRODUCTION AND BACKGROUND

The hetero-Diels−Alder (HDA) reaction of *C*-nitroso compounds provides an efficient entry to 1,2-oxazines (eq 1) and,

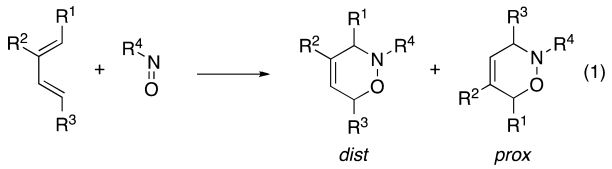

(1)

more generally, to 1,4-*N*,*O*-difunctional compounds via reductive cleavage of the *N*−*O* bond.[1−8] The reaction is of broad substrate scope, incorporating a variety of nitroso derivatives, including acyl−, aryl−, and imino−NO compounds, and variously substituted cyclic and acyclic dienes. Accordingly, the nitroso-HDA has been exploited in the total synthesis of various complex natural and unnatural products.[9−13] By employing chiral ligand−Cu^I, ligand−Ag^I, and ligand−Ru^{II} catalysts for the RNO-HDA reaction, variants of the reaction have been achieved with widely varying enantioselectivity, presumably via intermediate RNO−metal complexes.[14−17] A significant limitation of the RNO-HDA reaction, however, is its modest regioselectivity with some types of unsymmetrical dienes, especially with 1- and 2-alkyl dienes and 5-substituted cyclohexadienes (*proximal* vs *distal*, for R^2,R^3 = H; R^1,R^3 = H; eq 1).[14−16,18]

Houk et al. investigated computationally the mechanism and regioselectivities of the hetero-Diels−Alder reactions of nitroso compounds.[19−21] The HDA reaction of nitrosobenzene and butadiene was found to be concerted, but with a highly asynchronous transition state. Although it is not evident in the products, the *endo* path was calculated to be very strongly favored over the *exo* alternative due to repulsion between the diene and nitrogen's lone pair. A range of experimental regioselectivities were reproduced by the calculations and were found to hinge on a sensitive balance between FMO interactions, electrostatics, and steric effects.

Few studies designed to influence or control the regioselectivity of the nitroso-HDA reaction have been reported. Fragmentary results gathered from investigations of metal-catalyzed cycloadditions of *C*-nitroso dienophiles (mostly with LCu(I) catalysts) indicate that the regioselectivity with unsymmetrical dienes is sometimes different in the thermal (uncatalyzed) and catalyzed reactions.[4−13,22−26] A potentially complicating issue that can affect regioselectivity is the reaction's reversibility (i.e., thermodynamic control), a feature that has been demonstrated by Miller and co-workers in both higher temperature and LCu-catalyzed HDA reactions with nitroso−heteroarene reactants.[27] A novel approach to regio-

Received: April 6, 2014
Published: May 22, 2014

dx.doi.org/10.1021/jo5005907 | J. Org. Chem. 2014, 79, 5617−5626

control a *dist*-bicyclic ArNO/diene adduct (hapten) was employed to elicit a *dist*-selective antibody catalyst for the HDA reaction of nitrosobenzene and *cis*- and *trans*-1,3 pentadiene.[28,29]

The inspiration for our approach to regiocontrol in the nitroso-HDA reaction draws from both of the precedents cited above. In addition to the examples of enantioselective metal-catalyzed RNO-HDA reactions, the regioselectivity of other Lewis acid and transition-metal-catalyzed HDA reactions is strongly influenced by metal coordination.[30−32] We have developed a new method for catalyst selection based on the expected correlation between the binding affinity of transition-state analogues (TSAs) to a catalyst and the catalyst's activity and selectivity (Figure 1).[33] As applied to selectivity control, the use of regio- or stereoisomeric TSAs in a dynamic combinatorial templating process[34−39] could allow the elicitation of catalysts selective for the product derived from the TSA employed. In our recent work, we have demonstrated the viability and efficacy of the dynamic templating strategy for the elicitation of hydrolytic Zn catalysts.[40,41] In the present investigation, we examine the effects of copper catalysis on the regioselectivity of the HDA reaction between PyrNO and unsymmetrical dienes and evaluate both experimentally and computationally the efficacy of the dynamic templating approach for the elicitation of regioselective LCu(I) catalysts for this reaction.

2. RESULTS AND DISCUSSION

2.1. Uncatalyzed (Thermal) Reactions of PyrNO with Unsymmetrical Dienes. The reaction of PyrNO with excess 1,3-pentadiene (2:1 *E*/*Z* ratio) occurs rapidly at room temperature in methanol, leading to the formation of HDA adducts **1** in a 53:47 *prox*/*dist* ratio, which can be separated by HPLC (Scheme 1). Their structural assignment is based on 1D H NMR and 1D-NOE spectra and comparison with those reported previously.[12] Similarly, *E*,*E*-2,4-hexadienol (sorbyl alcohol) reacted with PyrNO in MeOH to produce a 35/65 *prox*/*dist* mixture of regioisomers **2**, whose structures were assigned based on their HMQC NMR spectra (Supporting Information). Interestingly, the regioselectivity in this reaction is solvent-dependent, for the same reaction run in CH_2Cl_2 produced a 10/90 *prox*/*dist* mixture. We suggest that the higher *dist* selectivity in CH_2Cl_2 is the result of stabilizing intramolecular H-bonding between the basic pyridine-*N* and the pendant −OH group in the *dist* HDA transition state. In methanol, MeOH−dienol and MeOH−pyridine H-bonding would compete to limit this *dist*-promoting interaction, leaving the regioselectivity to be largely determined by the inherently similar steric and electronic properties of the methyl and hydroxymethyl substituents. The uncatalyzed reaction of PyrNO with 1-phenyl-*E*-1,3-butadiene (rt, MeOH) results in selective formation of a single regioisomer that is assigned as the *prox*-isomer **3** based on 1D-NOE and HMQC NMR spectra as well as our computational analysis of the reaction (vide infra).

2.2. Computational Analysis of the Uncatalyzed PyrNO−Diene Reactions. *2.2.1. Reaction of PyrNO with 1,3-Pentadiene.* Eight possible concerted transition states for the reaction of 2-nitrosopyridine and (*E*)-1,3-pentadiene were computed using the M06 functional in Gaussian 09.[42] Geometry optimizations were performed with M06/6-31G(d) and the PCM[41] solvation model using MeOH as solvent. Single-point calculations were performed with M06/6-311+G-

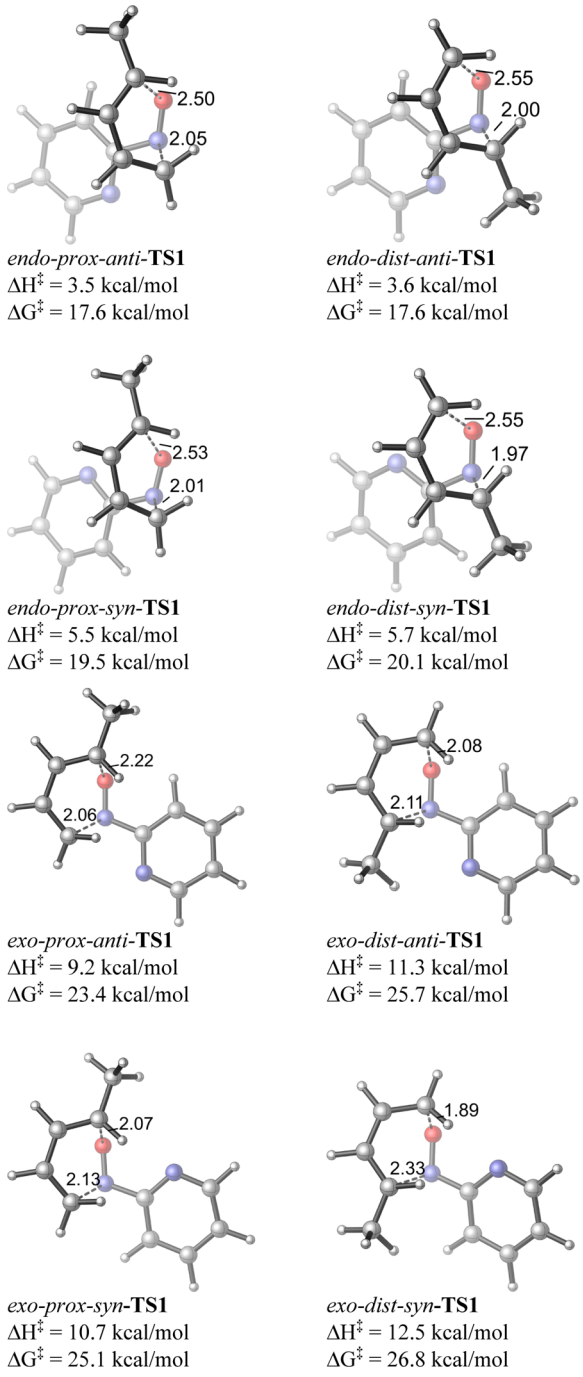

Figure 1. Calculated transition states for the 1,3-pentadiene/2-nitrosopyridine reaction.

(d,p) and the PCM solvation model.[43] For calculations with Cu catalysts (vide infra), the SDD effective core potential basis set was used for Cu. The N atom on the pyridine and the O atom on the nitroso unit may be *anti* or *syn*; the methyl on the pentadiene and the pyridine may be *distal* (*dist*) or *proximal* (*prox*); and the DA transition states may be *endo* or *exo*. The structures of the transition states, activation enthalpies, and free energies are summarized below. The most favorable transition states are *endo-dist-anti*-**TS1** and *endo-prox-anti*-**TS1**. Similar to the hetero-Diels−Alder reactions of other nitroso compounds, the *exo* transition states have much higher activation energies due to the *exo* lone pair effect. The *exo* transition states are destabilized by the four-electron repulsive interactions between

dx.doi.org/10.1021/jo5005907 | J. Org. Chem. 2014, 79, 5617−5626

Scheme 1. Uncatalyzed Diene−Nitrosopyridine Reactions

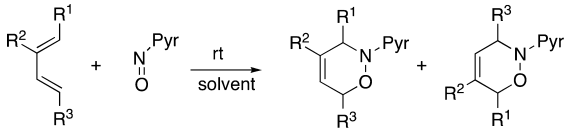

	Yield (%)	Selectivity (dist/prox)
R^1=CH_3, R^2=H, R^3=H (**1**)	82[a]	47/53
R^1=CH_2OH, R^2=H, R^3=CH_3 (**2**)	93[a]	66/34
	98[b]	90/10
R^1=C_6H_5, R^2=H, R^3=H (**3**)	45[a]	<5/>95

solvent = [a]MeOH; [b]CH_2Cl_2

the HOMO of the diene and the HOMO of the nitroso, i.e., the N and O lone pairs (Figure 2).[19−21] All *endo* transition states are highly asynchronous. The forming C−N and C−O bond lengths in all four *endo* transition states are similar, ∼2.0 and 2.5 Å, respectively. The higher energy *exo* transition states are less asynchronous with longer forming C−N bonds, a consequence of the repulsive HOMO−HOMO interactions between the nitrogen lone pair and the diene π orbital. High "twist-mode" asynchronicity[44,45] was also observed for the *endo* transition states. The diene is rotated 25−28° about the forming C−N bond. The twisted conformation presumably increases the overlap of the diene HOMO and the LUMO of the PyrNO (see Figure 2). The N atom on the pyridine and the O atom on the nitroso prefer to be *anti*. The *syn* transition states are 2−3 kcal/mol less stable. The most stable conformation of 2-nitrosopyridine is also *anti*. However, the *syn* conformer of 2-nitrosopyridine is only 0.3 kcal/mol less stable than its *anti* conformer. The greater *anti* preference in the transition state is attributed to the increasing repulsive interaction between the pyridine N and nitroso O lone pairs in the *anti* conformer, since the oxygen atom is more negatively charged in the highly asynchronous transition state than in the reactant. Thus, the regioselectivity is determined by the activation free energy difference between the most favorable *distal* transition-state *endo-dist-anti*-**TS1** and the most favorable *proximal* transition-state *endo-prox-anti*-**TS1**. They have essentially the same activation barriers. This agrees remarkably well with the low *distal*/*proximal* selectivities observed in the uncatalyzed reaction (Scheme 1).

We also tested the performance of different computational methods and the effects of solvation model in the computations (Table 1). The activation energies of the *distal* and *proximal* transition states are computed with B3LYP/6-31G(d) in the gas phase and in methanol solution with the PCM solvation model, and with M06/6-31G(d) in the gas phase. Only the most favorable *endoanti* pathways are considered. These results are compared with the M06/6-31G(d) results in solution (entries 4−6, Table 1). B3LYP overestimates the activation energies by 3−8 kcal/mol compared to the M06 results, as a result of the systematic error of B3LYP in treating π vs σ bonds.[42] B3LYP also slightly overestimates the regioselectivity, predicting that the *proximal* product is slightly favored. The gas phase activation energies and selectivities are very similar to those computed with the PCM solvation model. M06 single-point energy calculations with 6-311+G(d,p) and the larger 6-311++G(2d,p) basis set (entries 5 and 6) have very small effects on regioselectivities, both resulting in good agreement with the low regioselectivity in the experiment. The geometries and energies in the following discussions are all computed with M06/6-311+G(d,p)//M06/6-31G(d) using the PCM solvation model in methanol. For calculations with Cu catalyst, the SDD effective core potential basis set was used for Cu.

2.2.2. Reaction of PyrNO with 1-Phenylbutadiene. We also computed the eight possible concerted transition states for the hetero-Diels−Alder reaction of 2-nitrosopyridine and (*E*)-1-phenyl-1,3-butadiene with M06/6-311+G(d,p)//M06/6-31G(d) in methanol (see the Supporting Information for structures of all eight transition states). Similar to the reaction with (*E*)-1,3-pentadiene, the most favorable transition states are *endo-dist-anti*-**TS1** and *endo-prox-anti*-**TS1** (Figure 3). The *proximal* transition state is 3.7 kcal/mol more stable than the *distal* TS. This indicates high regioselectivity (>99%) for the *proximal* HDA product, in agreement with the experimentally observed complete *prox* regioselectivity. Both steric and electronic effects of the 1-phenyl substituent promote the *proximal* pathway, resulting in much greater regioselectivity than the reaction with pentadiene. The stronger electron-donating ability of the phenyl group leads to greater polarization of the HOMO of the diene to promote the frontier MO interaction with the PyrNO LUMO in the *distal* transition state. The bulkier phenyl group also increases the steric repulsions around the forming C−N bond in the *distal* transition state. Since the forming C−O bond is significantly longer than the C−N bond, the steric repulsions in the *distal* transition state is much weaker.

2.3. Cu(I)-Catalyzed Reactions of Pyr−NO with Unsymmetrical Dienes. In this our initial study of metal-catalyzed HDA regioselectivity, we chose $LCu(I)^+$ complexes as prospective catalysts, in part based on their reported efficacy for enantioselective HDA with coordinating RNO (R = 2-pyridyl).[14−21] Additionally, the typical ligand exchange lability of these d^{10} complexes[46−48] was thought to enable the timely establishment of equilibrium under mild conditions, desired for practical utilization of the dynamic templating process for

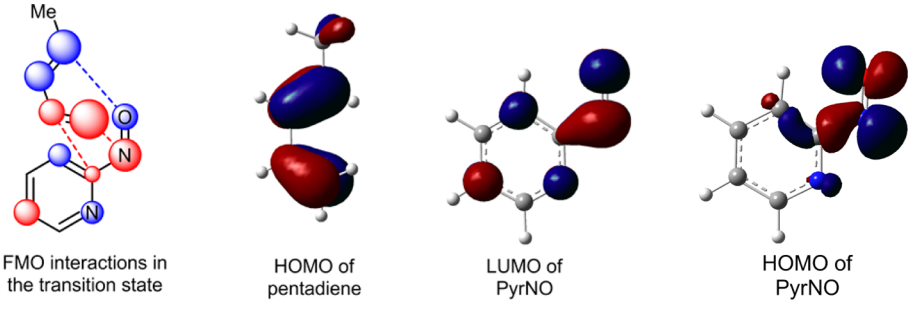

Figure 2. Frontier MOs of 1,3-pentadiene, 2-PyrNO, and the transition state.

dx.doi.org/10.1021/jo5005907 | J. Org. Chem. 2014, 79, 5617−5626

Table 1. Activation Barriers for the Reaction of 2-Nitrosopyridine and (*E*)-1,3-Pentadiene

entry	method	$\Delta G^{\ddagger}$ ($\Delta H^{\ddagger}$)-*proximal*	$\Delta G^{\ddagger}$ ($\Delta H^{\ddagger}$)-*distal*	$\Delta\Delta G^{\ddagger}$ ($\Delta\Delta H^{\ddagger}$)-*dist−prox*
1	B3LYP/6-31G(d) gas	21.4 (7.9)	22.7 (8.7)	1.3 (0.8)
2	B3LYP/6-31G(d)-PCM	21.3 (7.8)	23.0 (9.0)	1.7 (1.1)
3	M06/6-31G(d) gas	15.1 (1.3)	15.3 (0.8)	0.2 (−0.5)
4	M06/6-31G(d)-PCM(MeOH)	15.3 (1.2)	15.1 (1.1)	−0.2 (−0.1)
5	M06/6-311+G(d,p)-PCM//M06/6-31G(d)-PCM(MeOH)	17.6 (3.5)	17.6 (3.6)	0.0 (0.1)
6	M06/6-311++G(2d,p)-PCM//M06/6-31G(d)-PCM(MeOH)	18.2 (4.1)	18.3 (4.3)	0.1 (0.2)

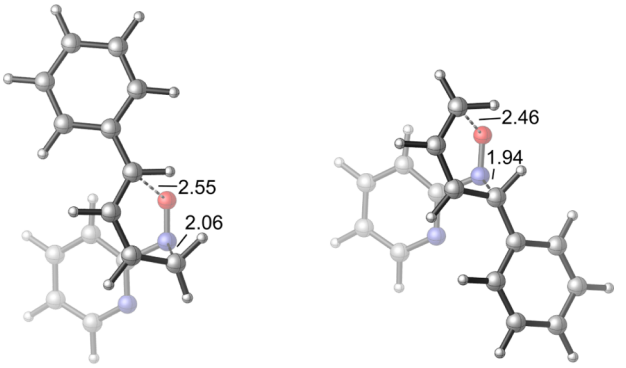

endo-prox-anti-**TS1-Ph**
$\Delta H^{\ddagger}$ = 2.8 kcal/mol
$\Delta G^{\ddagger}$ = 17.1 kcal/mol

endo-dist-anti-**TS1-Ph**
$\Delta H^{\ddagger}$ = 6.2 kcal/mol
$\Delta G^{\ddagger}$ = 20.8 kcal/mol

Figure 3. Calculated transition states for the phenylbutadiene/nitrosopyridine reaction.

catalyst selection. Two classes of LCu(I) complexes were employed as prospective catalysts, $Cu(AN)_4^+$ (AN = CH_3CN) and L_2Cu^+, in which L = bidentate imine. The latter were produced by combining heteroaromatic aldehydes with primary amines (Figure 4), individually or in sets (libraries), to form the corresponding bidentate imine ligands and then reacting these with $Cu(AN)_4^+$ (Scheme 2). Visual and ESI-MS monitoring of these reactions allows ready detection of L_2Cu^+ species by the distinctive Cu isotope pattern (see the Supporting Information), which indicates that equilibrium is achieved within 24 h at room temperature. Generally, the individual complexes were not isolated but rather were generated and used in situ.

In order to establish the composition and accurately determine the structure of a representative L_2Cu^+ complex, the compound **28** derived from 2-quinolinecarboxaldehyde (**25**) and 1-adamantylmethylamine (**6**) was prepared (eq 2)

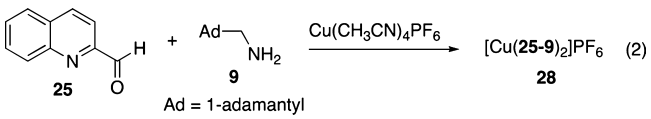

(2)

and structurally characterized by X-ray diffraction (Figure 5). The slightly distorted tetrahedral geometry about Cu is apparent from the selected Cu−N and N−Cu−N angles (see the Supporting Information). It is presumed (supported by MS and computational analysis, vide infra) that the coordinatively saturated L_2Cu^+ species catalyze the HDA reaction with PyrNO by dissociating one L and coordinating PyrNO in a bidentate fashion.

The Cu-catalyzed PyrNO/diene reactions were carried out by combining the preformed $Cu(diimine)_2^+$ complex or $Cu(AN)_4^+$ with PyrNO, followed by the addition of the diene, typically at rt in MeOH. Mixing the components at lower

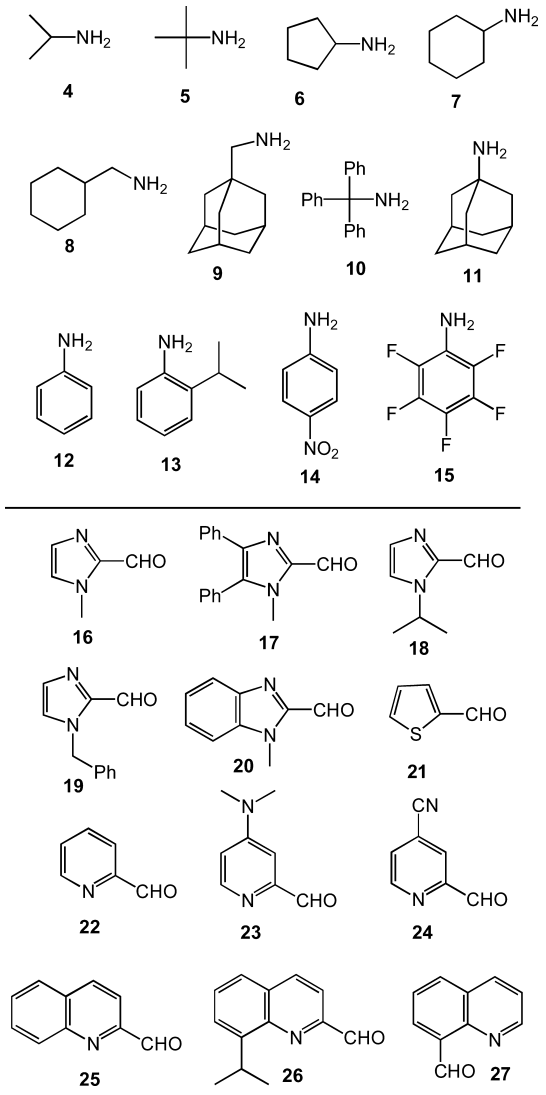

Figure 4. Amines and aldehydes for producing imine ligands.

Scheme 2. Imine Ligand Formation and Complexation

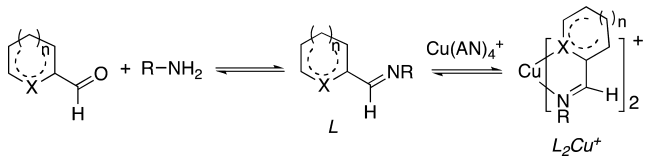

temperature, e.g., −78 °C, at which the uncatalyzed reactions are slow, and warming to room temperature had little effect on regioselectivity, indicating that the background reaction contributes little to the regioselectivity and that the selectivity was kinetically determined. This was further supported by showing that the individual regioisomers did not isomerize in

dx.doi.org/10.1021/jo5005907 | J. Org. Chem. 2014, 79, 5617−5626

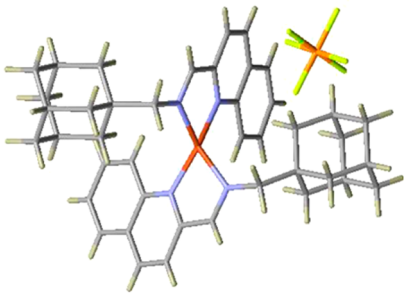

28

Figure 5. X-ray determined structure of $[Cu(\mathbf{25}-\mathbf{9})_2]^+$ (**28**) (see the Supporting Information). Atom key: Cu = red, C = gray, N = blue, P = orange, F = yellow).

the presence of catalyst at room temperature. The regioselectivity results for the pentadiene/PyrNO reaction with $Cu(AN)_4^+$ and selected L_2Cu^+ catalysts are summarized in Scheme 3.

Scheme 3. Regioselectivity in the Cu-Catalyzed Diene/PyrNO Reactions[a,b,c,d]

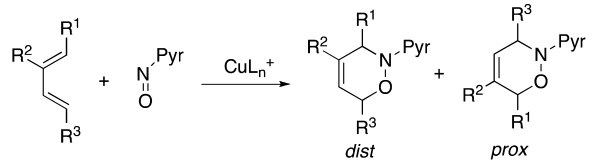

diene	*cat*	*Yield(%)*	*selectivity (dist/prox)*[a]
R^1=CH_3; R^2,R^3=H	$Cu(AN)_4^+$	82	90:10 (47:53)[b]
	Cu(diimine)$^{+c}$	55[d]	35-45:65-55[c]
R^1=Ph; R^2,R^3=H	$Cu(AN)_4^+$	30	<5 : >95 (<5:>95)[b]
R^1=CH_2OH, R^2=H, R^3=CH_3	$Cu(AN)_4^+$	35	50:50 (66:34)[b]

[a]Solvent = MeOH. [b]Uncatalyzed regioselectivity. [c]Diimine from RCHO (**4**–**15**) + RNH_2 (**16**–**27**). [d]Diimine **22**–**7**.

The regioselectivity of the Cu-catalyzed reactions was most dramatically affected with $Cu(AN)_4PF_6$ as the catalyst, providing a 10:90 *prox*/*dist* selectivity, improved substantially over the uncatalyzed reaction. More than 25 $(diimine)_2Cu^+$ complexes, generated from condensation of the primary amines **4**–**15** with heterocyclic aldehydes **16**–**27**, were also tested for their effects on the *prox*/*dis* regioselectivity of the PyrNO/diene reaction (10 mol %, MeOH solvent, rt; see the Supporting Information). In all cases that were evaluated, the resulting HDA adducts were produced with modest regioselectivities, slightly favoring the *proximal* regioisomer, e.g., 65–55%(*prox*):35–45%(*dist*). Despite the diversity of electronic and steric effects anticipated from this set of imine ligands and complexes, it is somewhat surprising that the effects on regioselectivity were rather limited. This issue is considered further in our computational analysis of the Cu-catalyzed reactions.

Evaluation of the Cu-catalyzed regioselectivity for the PyrNO/sorbyl alcohol (R^1 = CH_2OH, R^2 = H, R^3 = CH_3) reaction was limited to determining the reaction regioselectivity with $Cu(AN)_4^+$ and $(\mathbf{22}-\mathbf{7})_2Cu^+$ as catalysts (MeOH, 10 mol % cat, rt). The *prox*/*dist* selectivities measured were 50:50 and 34:66 respectively (Scheme 3). Relative to the uncatalyzed reaction, the former is modestly more *prox* selective, whereas the latter has the same selectivity as the uncatalyzed reaction. Thus, CuL– effects are modest for this nearly electronically symmetrical substrate. We evaluated whether Cu(I) catalysis of the phenylbutadiene/PyrNO reaction could override the highly *prox* selective uncatalyzed regioselectivity. Conducting the reaction in the presence of $Cu(AN)_4^+$ (highly *dist* selective for 1-Me-butadiene), however, still only afforded the *prox* product.

2.4. MS Binding Studies: Binary and Ternary Complexes. To probe for potential intermediate complexes for catalysis/regiocontrol and to evaluate the efficacy of catalyst selection by dynamic templating, we investigated the composition of equilibrating mixtures of binary L_2Cu^+ complexes and their response to the addition of isomeric "product-like" *pro*-transition state analogues (TSAs) to form LCu(*prox*-TSA)$^+$ and LCu(*dist*-TSA)$^+$ (Scheme 4). Mixing 2-quinolinecarboxaldehyde (**25**) and a set of primary amines, cyclohexylamine (**7**), 1-cyclohexylmethylamine (**8**), and 1-adamantylmethylamine (**9**), together with $Cu(AN)_4^+$ in MeOH produces a library of all six possible $(diimine)_2Cu^+$ complexes whose composition can be established by ESI-MS analysis (e.g., Figure 6a and the Supporting Information); the relative abundance of species is constant (has reached equilibrium) within 72 h at rt.

To elicit Cu complexes that mimic the regioisomeric transition states for the cycloaddition of pentadiene with PyrNO, we chose the isomeric *prox* and *dist* adducts as "late" *pro*-TSAs (**1**). ESI-MS analysis of the mixtures obtained upon addition of 100 equiv of either isomeric TSA to the library of quinoline-based L_2Cu^+ (above) confirmed the formation of LCu(TSA)$^+$ by detection of the molecular ions with the distinctive copper isotope pattern (Figure 6). Significant differences can be seen in the relative abundance of the isomeric LCu(TSA)$^+$ present in the two libraries produced from the isomeric TSAs, showing the ability of the LCu^+ species to discriminate between the isomeric TSAs. This selectivity was quantitatively assessed by comparing the integrated ion intensities of the ternary LCu(TSA)$^+$ complexes produced by treating the same set of L_2Cu^+ complexes (L = **25**–**7**, **25**–**8**, **25**–**9**) with the two regioisomeric TSAs,

Scheme 4. Formation of L_2Cu^+ and LCu(TSA)$^+$ Complexes

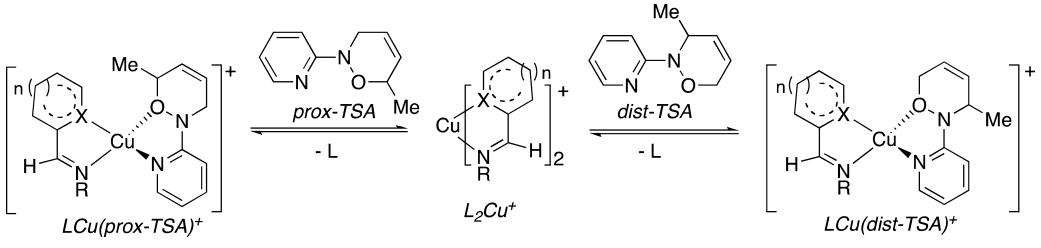

dx.doi.org/10.1021/jo5005907 | J. Org. Chem. 2014, 79, 5617–5626

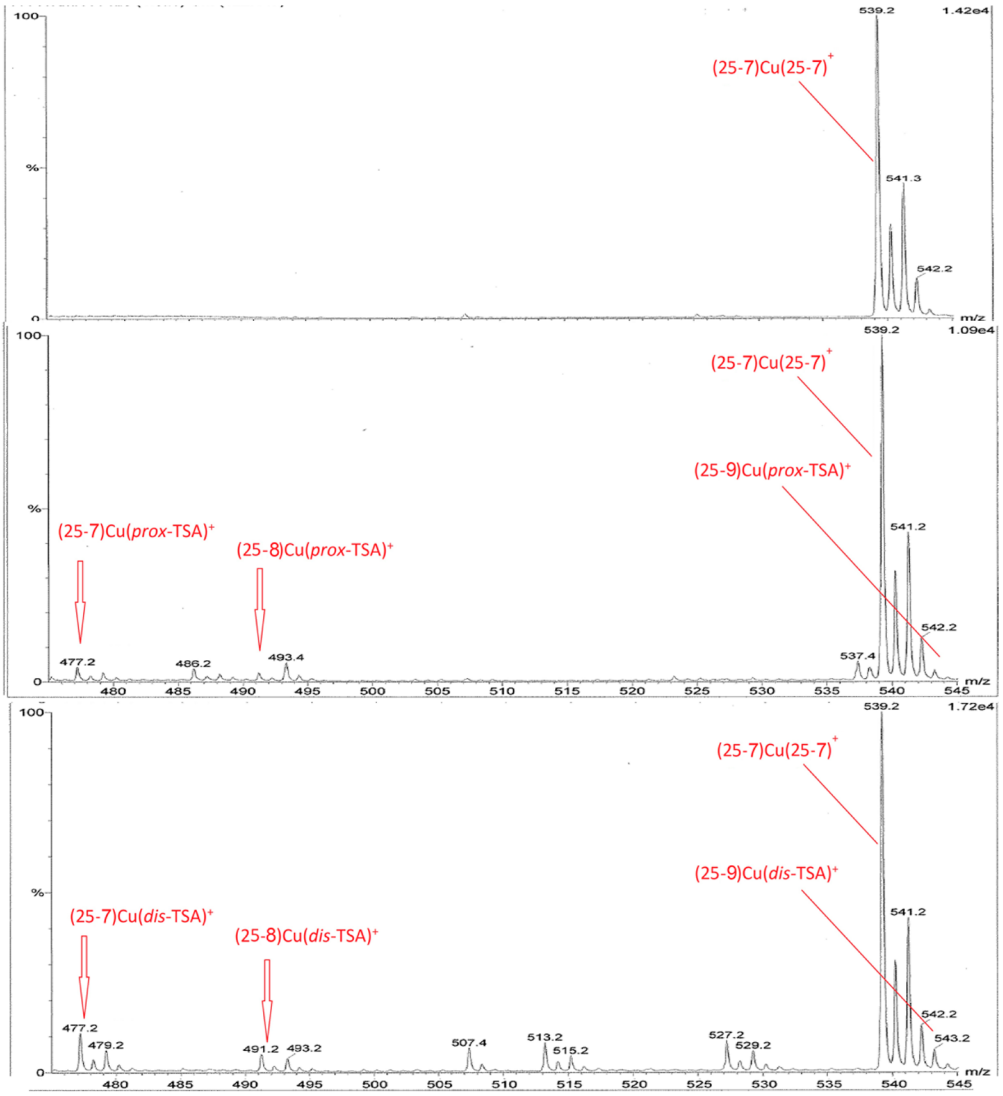

Figure 6. ESI-Mass spectra of (a) **25** + **7** + **8** + **9** + $Cu(AN)_4^+$; (b) L_2Cu^+ + *prox*-TSA (**1**); and (c) L_2Cu^+ + *dist*-TSA (**1**).

normalized to the signal from the internal standard tetrabutylammonium hexafluorophosphate (m/z = 242). Since the isomeric LCu(*prox*-TSA)$^+$ and LCu(*dist*-TSA)$^+$ complexes are structurally and electronically similar, their ionizabilities are likely to be comparable. The MS binding *prox*/*dist* ratios were thus determined for each of the ternary LCu(TSA)$^+$ and compared with the regioisomeric product selectivity in the L_2Cu-catalyzed reactions of PyrNO with 1,3-pentadiene (Figure 7). The correlation between the TSA binding selectivity and the catalytic reaction's product selectivity is judged to be marginal given the small spread of observed *prox*/*dist* selectivities, the experimental error of the MS measurements, and the relatively small data set (see the Supporting Information).

2.5. Computational Analysis of the Cu-Catalyzed Reactions. *2.5.1. Cu(AN)$_2^+$-Catalyzed Reaction of PyrNO and Pentadiene.* To explore the effects of Cu catalysts on the regioselectivity and the origin of difference of regioselectivities with $Cu(AN)_2^+$ and Cu(diimine)$^+$ in the PyrNO/pentadiene reactions, we performed a computational study with the M06 functional. Geometry optimizations were performed with M06/6-31G(d) and the PCM solvation model using MeOH as solvent. Single-point calculations were performed with M06/6-311+G(d,p) and the PCM solvation model. The SDD effective core potential basis set was used for Cu in geometry optimizations and single-point energy calculations. The most favorable transition states leading to the *distal* and *proximal*-products in the $Cu(AN)_2^+$-catalyzed reaction of PyrNO and pentadiene are shown in Figure 8. Similar to the uncatalyzed reaction, the *endo* transition states are more stable than the *exo* TS. The Cu binds to the pyridine N atom and the nitroso O atom; i.e., the nitrosopyridine adopts the *syn* conformation.

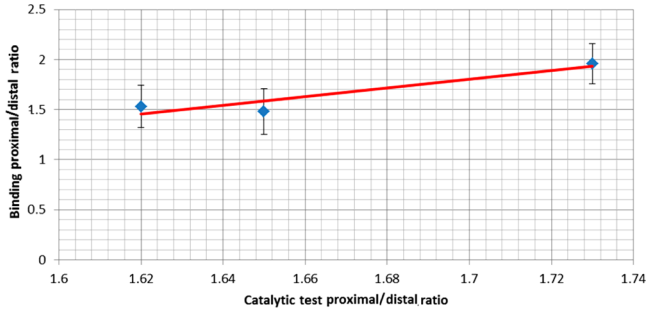

Figure 7. Correlation of ESI-MS LCu-TSA binding selectivity and catalytic product selectivity.

dx.doi.org/10.1021/jo5005907 | J. Org. Chem. 2014, 79, 5617−5626

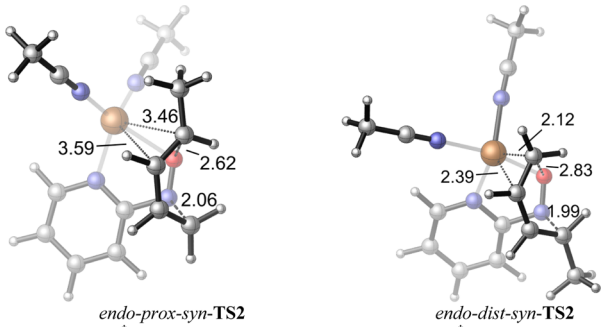

Figure 8. Calculated transition states for the $(AN)_2Cu^+$-catalyzed PyrNO/pentadiene reaction.

This is in contrast to the *anti* conformation in the uncatalyzed reaction. The activation free energies and enthalpies were computed with respect to the separated reactants: pentadiene and the PyrNO−$Cu(AN)_2^+$ complex. Both the *distal* and the *proximal* transition states have lower activation barriers than those in the uncatalyzed reaction. The *distal* transition state (*endo-dist-syn*-**TS2**) is 1.6 kcal/mol more stable than the *proximal* TS (*endo-prox-syn*-**TS2**), in agreement with the experimental selectivity for the *distal* product. Binding with $Cu(AN)_2^+$ lowers the LUMO of PyrNO from −3.38 to −3.92 eV. Thus, the increase of reactivity with Cu catalysts can be attributed to better FMO interactions between the HOMO of the diene and the lowered LUMO of the dienophile, similar to Lewis acid catalysis.[49] However, the high *distal* selectivity with the $Cu(AN)_2^+$ catalyst cannot be simply explained by the Lewis acid catalysis mechanism. Lewis acid coordination typically induces further polarization of the dienophile LUMO and thus affects regioselectivity. In contrast, the Cu catalyst binds bidentate to the conjugated PyrNO substrate. This leads to minimal changes of the LUMO coefficients on the N and O atoms of PyrNO (Figure 9). Indeed, the lower activation

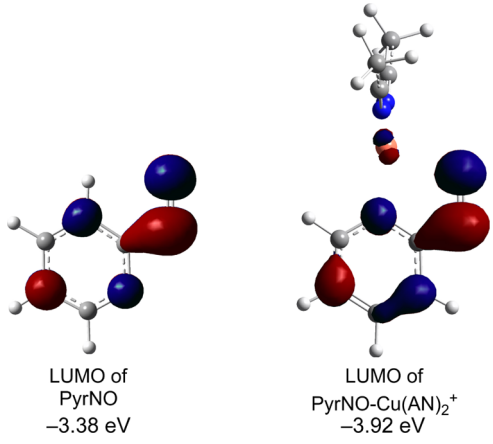

Figure 9. LUMOs of PyrNO and $(PyrNO)Cu(AN)_2^+$.

energy of the *distal* transition-state *endo-dist-syn*-**TS2** is due to the binding of Cu to one of the C=C double bonds in pentadiene. Such binding is expected to be relatively weak, since the Cu in the PyrNO−$Cu(AN)_2^+$ complex already has 18 valence electrons. Nonetheless, the short Cu−C1 and Cu−C2 distances (2.12 and 2.39 Å, respectively) indicate stabilizing π interactions in the *distal* transition state. Because of the Cu coordination, the *distal* transition state becomes more asynchronous. The forming C−O bond in *endo-dist-syn*-TS2 is 2.83 Å, significantly longer than those in the *proximal* transition state and the uncatalyzed transition states (2.5−2.6 Å). In contrast, in the *proximal* transition state *endo-prox-syn*-**TS2**, the Cu does not bind to the pentadiene C3=C4 double bond. This is due to the greater steric repulsions and less nucleophilicity of the internal C4 carbon on pentadiene.

2.5.2. Cu(diimine)$^+$-Catalyzed Reaction of PyrNO and Pentadiene. We then computed the transition states in the Cu(diimine)$^+$-catalyzed reaction of PyrNO and 1,3-pentadiene with diimine **5**−**16** as the ligand in the calculations. Experimentally, the (**5**−**16**)Cu-complex produces a 60:40 *prox*:*dist* regioselectivity (see the Supporting Information). The most favorable transition states leading to the *distal* and *proximal* products in the Cu(**5**−**16**)$^+$-catalyzed reaction are shown in Figure 10. The geometries and the forming C−X

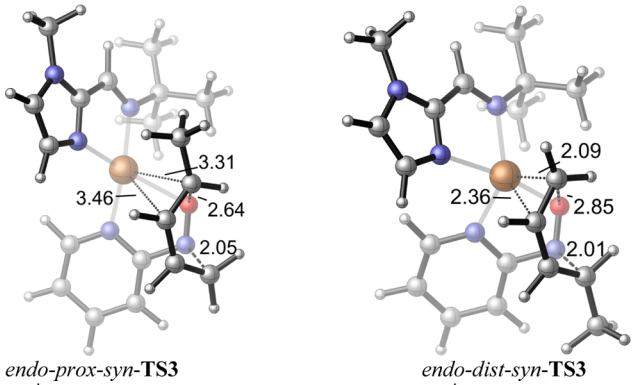

Figure 10. Calculated transition states for the $(\mathbf{5}-\mathbf{16})_2Cu^+$-catalyzed PyrNO/pentadiene reaction.

bond lengths of the transition states are very similar to those with the $Cu(AN)_2^+$ catalyst. The *endo* transition states are more stable than the *exo* TS. Cu binds to the pyridine N atom and the nitroso O atom. The bulky *t*-Bu group on the diimine ligand prefers to point away from the pyridine. Similar to the transition states with the $Cu(AN)_2^+$ catalyst, the Cu binds to the diene π bond in the *distal* TS, whereas no such Cu−diene binding is observed in the *proximal* TS. However, such Cu−diene binding does not promote the *distal* pathway to the same extent as in the $Cu(AN)_2^+$-catalyzed reaction. The *proximal* TS with Cu(**5**−**16**)$^+$ is 0.9 kcal/mol more stable than the *distal* TS in terms of Gibbs free energies. The predicted selectivity is lower than that in the reaction with $Cu(AN)_2^+$ in which the *distal* TS is favored by 1.6 kcal/mol. This is in agreement with the decreased regioselectivity observed in the experiment with Cu(**5**−**16**)$^+$. The diminished selectivity for the *distal* product is presumably due to the less favorable Cu−diene binding in the *proximal* transition state when employing the more electron-rich and bulkier diimine ligand.

Experimentally, the regioselectivity of the reaction of PyrNO and 1,3-pentadiene is minimally affected by the choice of diimine ligands. The computed transition-state structures also suggest that the steric and electronic properties of the ligand should have small effects on the relative energies of *distal* and *proximal* transition states. First of all, the pseudotetrahedral geometry of Cu orients the diimine ligand almost parallel to the

dx.doi.org/10.1021/jo5005907 | J. Org. Chem. 2014, 79, 5617−5626

diene. Both substituents on the diimine ligand are pointing away from the terminal methyl group in *endo-prox-syn*-**TS3**. The orientation of the ligand and the long forming C−O bond prevent any ligand−substrate steric repulsions with the methyl substituent on the diene. As described above, electronic properties of the ligand will not affect the degree of polarization of the nitroso LUMO, and the electronic effects on the Cu−diene binding in the *proximal* TS are also expected to be small since such binding is very weak when diimine ligands are employed. These suggest that the electronic effects on regioselectivities are small.

3. CONCLUSIONS

The uncatalyzed reactions of nitrosopyridine with pentadiene or sorbyl alcohol occur with low regioselectivity (*prox*:*dist* 53:47, 34:66), whereas that with 1-phenylbutadiene proceeds with complete *prox* selectivity. Computational analysis of the pentadiene/PyrNO reaction finds no energy difference (0.0 kcal/mol) between the most stable transition states, leading to nearly equal amounts of *prox* and *dist* cycloadducts, in agreement with experiment. The *proximal* transition state is strongly favored (3.7 kcal/mol) over the *distal* for the phenylbutadiene/PyrNO reaction, in accord with the high selectivity observed. The regioselectivity of the pentadiene/PyrNO reaction is improved markedly (10:90 *prox*/*dist*) in the presence $Cu(CH_3CN)_4^+$, whereas various $(diimine)_2Cu^+$ catalysts increase selectivity for the *proximal* product (55−65%). Modest effects of the catalyst nature on regioselectivity are observed in the sorbyl alcohol and 1-phenylbutadiene reactions. Transition states in the $Cu(AN)_4^+$- and $Cu(diimine)_2^+$-catalyzed reactions of PyrNO with pentadiene involve coordinated PyrNO and the diene, which account for the observed regioselectivities in the Cu-catalyzed reactions. Coordination effects on the regioselectivity are derived from FMO orbital interactions and the extent of electron transfer between the Cu center and the coordinated nitroso and diene units. A marginal correlation was found between the relative affinity of a set of $(diimine)_2Cu^+$ complexes for the *prox* and *dist* cycloadducts and the *prox*/*dist* product regioselectivity produced by the corresponding complex catalysts. New classes of metal complex catalysts are being investigated, which are expected to transmit regio-orienting steric and electronic effects more effectively to the coordinating *C*-nitroso and diene units.

4. EXPERIMENTAL SECTION

4.1. General. Unless otherwise noted, all solvents were predried in a solvent still (MeOH dried over Mg, CH_2Cl_2 and acetonitrile dried over CaH_2), distilled, and then freeze−pump−thawed for at least five cycles. The following compounds were prepared according to the cited procedures and identified by comparison of their ^{1}H NMR spectra with those reported: 2-nitrosopyridine,[50] and 1-phenyl-1,3-butadiene.[51]

4.2. Preparation of 3-Methyl-2-(pyridin-2-yl)-3,6-dihydro-2*H*-1,2-oxazine (*Distal* 1) and 6-Methyl-2-(pyridin-2-yl)-3,6-dihydro-2*H*-1,2-oxazine (*Proximal* 1). 2-Nitrosopyridine (0.216 g, 2.0 mmol) was dissolved in 100 mL of methanol, followed by the addition of 1 mL of 1,3-pentadiene (ca. 6 mmol, 75% pure, 2:1 *E*/*Z*). The solution was left for 1 h, and then the solvent was removed in vacuo to leave a brown liquid mixture. Column chromatography of the liquid over silica gel with 7:3 hexane:diethyl ether gave 0.295 g (84%) of a light yellow liquid. The ratio of *proximal*/*distal* isomers was 46:54 (NMR integration).

A few reaction mixtures were combined to give 1.4 g of the regioisomeric mixture (8.0 mmol). Twenty-five μL of the reaction product mixture was separated on a C18 Bakerbond column (22.5 × 250 mm) using 4:6 MeOH:H_2O at 16 mL/min (UV detection at 267 nm). Fraction 1 was collected from 19.5 to 21.4 min and fraction 2 from 23.9 to 25.4 min. After multiple injection/collection cycles, each combined fraction was concentrated to 40% of the original volume and then saturated with NaCl. Each fraction was extracted three times with 200 mL of Et_2O, and then the combined organic layers were dried over $MgSO_4$ and concentrated in vacuo to yield 0.341 g of *dist* adduct in fraction 1 (1.94 mmol; from 4.32 mmol calculated in the original mixture by H NMR analysis, 45% yield) and 0.261 g of the *prox* isomer in fraction 2 (1.48 mmol; from 3.68 mmol calculated in the original mixture by H NMR analysis, 40% yield) from 1.4 g (8.0 mmol) of the thermal product mixture.

4.2.1. 3-Methyl-2-(pyridin-2-yl)-3,6-dihydro-2H-1,2-oxazine (Distal 1). ^{1}H NMR (300 MHz, $CDCl_3$): δ 8.22 (dd, *J* = 5.1, 1.2 Hz, 1H), 7.58 (dt, *J* = 7.8, 1.8 Hz, 1H), 7.1 (d, *J* = 7.8 Hz, 1H), 6.75 (t, *J* = 6 Hz, 1H) 5.98 (ddd, *J* = 9.0, 4.2, 1.8 Hz, 1H), 5.83 (ddd, *J* = 11.7, 3.6, 1.8 Hz, 1H), 4.83 (m, 1H), 4.64 (ddd, *J* = 17.7, 6.6, 2.4 Hz, 1H), 4.3 (ddd, *J* = 15.3, 6.6, 1.8 Hz, 1H), 1.21 (d, *J* = 6.6 Hz).

4.2.2. 6-Methyl-2-(pyridin-2-yl)-3,6-dihydro-2H-1,2-oxazine (Proximal 1). ^{1}H NMR (300 MHz, $CDCl_3$): δ 8.23 (dd, *J* = 4.8, 1.8 Hz, 1H), 7.59 (dt, *J* = 7.2, 2.4 Hz, 1H), 7.20 (d, *J* = 8.4 Hz, 1H), 6.80 (t, *J* = 6 Hz, 1H) 5.96 (ddd, *J* = 7.5, 5.7, 1.8 Hz, 1H), 5.83 (m, 1H), 4.73 (m, 1H), 4.36 (dquin, *J* = 17.1, 2.4 Hz, 1H), 3.95 (ddd, *J* = 17.1, 4.8, 2.4 Hz, 1H), 1.34 (d, *J* = 6.9 Hz). 2D/NOE NMR data for the regioisomeric adducts in the Supporting Information.

4.3. Preparation of (6-Methyl-2-(pyridin-2-yl)-3,6-dihydro-2*H*-1,2-oxazin-3-yl)methanol (*Distal* 2) and (3-Methyl-2-(pyridin-2-yl)-3,6-dihydro-2*H*-1,2-oxazin-6-yl)methanol (*Proximal* 2). 2-Nitrosopyridine (216 mg, 2.00 mmol) was dissolved in 100 mL of methanol, followed by the addition of 196 mg (2.00 mmol) of sorbyl alcohol. The solution was left for 1 h, and then the solvent was removed in vacuo to leave a brown liquid mixture. Column chromatography of the liquid over silica gel 1:1 hexane:ethyl acetate gave 383 mg (93%) of a light yellow liquid. The *proximal*/*distal* ratio of adducts was 66:34 (NMR). Column chromatography of the liquid above with 98/2 CH_2Cl_2/MeOH separated the two products.

4.3.1. (6-Methyl-2-(pyridin-2-yl)-3,6-dihydro-2H-1,2-oxazin-3-yl)-methanol (Distal 2). ^{1}H NMR (500 MHz, $CDCl_3$): δ 8.15 (dd, *J* = 5.0, 1.7 Hz, 1H), 7.59 (dt, *J* = 7.8, 7.8, 1.7 Hz, 1H), 7.12 (dd, *J* = 7.9, 1.0 Hz, 1H), 6.76 (ddd, *J* = 7.9, 5.0, 1.0 Hz, 1H), 5.92 (ddd, *J* = 10.5, 4.5, 2.0 Hz 1H), 5.83 (dt, *J* = 10.5, 1.6 Hz, 1H), 5.04 (m, 1H), 4.61 (m, 1H), 3.89 (dd, *J* = 11.6, 7.1 Hz, 1H), 3.81 (dd, *J* = 11.6, 3.3 Hz, 1H), 1.31 (d, 6.7 Hz, 3H). ^{13}C NMR (125 MHz, $CDCl_3$): 159.86, 147.47, 138.21, 131.18, 124.02, 116.07, 110.22, 71.16, 64.04, 56.50, 19.09. HRMS (ESI) calc for $C_{11}H_{15}N_2O_2$ ($M + H^+$) 207.1133, found 207.1130; calc for $C_{11}H_{14}N_2O_2Na$ ($M + Na^+$) 229.0953, found 229.0947. For 2D/NOE NMR data, see the Supporting Information.

4.3.2. (3-Methyl-2-(pyridin-2-yl)-3,6-dihydro-2H-1,2-oxazin-6-yl)-methanol (Proximal 2). ^{1}H NMR (500 MHz, $CDCl_3$): δ 8.24 (dd, *J* = 5.06, 1.8 Hz, 1H), 7.58 (dt, *J* = 7.8, 7.8, 1.8 Hz, 1H), 7.10 (d, *J* = 7.8 Hz, 1H), 6.77 (dd, *J* = 7.8, 5.06 Hz, 1H), 6.10 (ddd, *J* = 10.2, 4.8, 2.1 Hz, 1H), 5.70 (dt, *J* = 10.2, 1.3, 1H), 4.88 (m, 1H), 4.73 (m, 1H), 3.85 (dd, *J* = 12.2, 6.5 Hz, 1H), 3.76 (dd, *J* = 12.2, 6.5 Hz, 1H), 1.24 (d, *J* = 6.7 Hz, 3H). ^{13}C NMR (125 MHz, $CDCl_3$): 159.78, 147.91, 137.93, 132.11, 123.98, 116.06, 109.93, 78.04, 64.27, 51.47, 16.22. HRMS (ESI) calc for $C_{11}H_{15}N_2O_2$ ($M + H^+$) 207.1133, found 207.1130; calc for $C_{11}H_{14}N_2O_2Na$ ($M + Na^+$) 229.0953, found 229.0947. 2D/NOE NMR data in the Supporting Information.

4.4. Preparation of 6-Phenyl-2-(pyridin-2-yl)-3,6-dihydro-2*H*-1,2-oxazine (*Proximal* 3). 2-Nitrosopyridine (216 mg, 2.00 mmol) was dissolved in 100 mL of methanol, followed by the addition of 260 mg of 1-phenylbutadiene. The solution was left for 1 h, and then the solvent was removed in vacuo to leave a brown liquid mixture. Column chromatography of the liquid over silica gel with 6:4 hexane:diethyl ether gave 214 mg (45%) of light yellow liquid.

^{1}H NMR (500 MHz, $CDCl_3$): δ 8.23 (dd, *J* = 4.6, 1.8 Hz, 1H), 7.54 (dt, *J* = 7.9, 1.8 Hz, 1H), 7.50 (m, 2H), 7.39 (m, 2H), 7.14 (d, *J* = 7.9, 1H), 6.80 (dd, *J* = 7.9, 4.6 Hz), 6.21 (m, *J* = 10.4 Hz, 1H), 6.05 (m, *J* = 10.4 Hz, 1H), 5.62 (m, 1H), 4.48 (m, *J* = 17.2 Hz, 1H), 4.15 (m, *J* = 17.2 Hz, 1H). ^{13}C NMR (125 MHz, $CDCl_3$): 160.9, 147.3, 138.6, 137.5, 128.5, 128.3, 128.1, 124.4, 116.6, 110.4, 79.8, 47.7. HRMS (ESI)

dx.doi.org/10.1021/jo5005907 | J. Org. Chem. 2014, 79, 5617−5626

calc for $C_{15}H_{15}N_2O$ ($M + H^+$) 239.1185, found 239.1185. 2D/NOE NMR data provided in the Supporting Information.

4.5. Preparation of Copper(2-quinoline-1-methyl-adamantyl-imine)$_2$ Hexafluorophosphate (28). In a drybox, 37 mg (0.10 mmol) of tetrakis(acetonitrile)copper(I) hexafluorophosphate was dissolved in 1.0 mL of methanol. In a different vial, 31 mg (0.20 mmol) of 2-quinolinecarboxaldehyde and 32 μL (0.20 mmol) of 1-adamantylmethylamine were added to 1 mL of methanol. The vial was shaken vigorously to partially dissolve the reactants, and the solutions from the two vials were mixed to form a purple red solution. After 24 h, the dark purple crystals were taken out of the drybox and carefully washed with cold acetone. The crystals appear to be air-stable. ^{1}H NMR (300 MHz, $CDCl_3$): δ 9.00 (s, 1H), 8.61 (d, J = 8.1 Hz, 1H), 8.13 (d, J = 8.1 Hz, 1H), 7.95 (dd, J = 5.4, 2.4 Hz, 1H), 7.59 (m, 3H), 2.62 (b, 3H), 1.85 (b, 6H), 1.57 (m, b, 8H). See the Supporting Information for NMR spectrum and details of X-ray crystal structure determination.

4.6. ESI-MS Quantification of the LCu(TSA)$^+$ Complex Library. In a drybox, 37 mg (0.10 mmol) of tetrakis(acetonitrile)-copper(I) hexafluorophosphate was dissolved in 1.0 mL of methanol. In a different vial, the imine ligands were formed by adding 1 equiv (0.10 mmol) of 2-quinolinecarboxaldehyde (16 mg), cyclohexylamine (12 μL), cyclohexylmethyl amine (13 μL), and 1-adamantylmethyl amine (18 μL) and diluting with methanol to make 1.0 mL total volume. A red brown solution was formed upon mixing the imine- and copper-containing solutions; the resulting solution was left overnight to reach equilibrium. On the next day, 80 μL of the above solution and 10 μL of tetrabutylammonium hexafluorophosphate (0.0010 mmol) were combined and diluted with CH_3OH to make a 4 mL stock solution. In two different septa-capped vials, 1 mL of the stock solution was added to each vial, followed by 16 μL (0.10 mmol) of the *distal* or the *proximal* adduct TSA. The mixtures were left in the drybox for 72 h to reach equilibrium. Without further dilution, the mixtures were injected to overfill a 20 μL sample loop under a flow of methanol (1 mL/min). A Micromass Q-TOF mass spectrometer was used for analysis with a capillary voltage set at 3000 V. The ion integration was measured with the most abundant isotopomer of each complex using the built-in program. Each sample was injected into the mass spectrometer five times, and the resulting mass spectra were acquired and the ion integrations were determined. The binding ratio of the isomers was determined by averaging the integrated ion count of each regioisomeric ternary complex. The tetrabutylammonium ion (m/z = 242) was monitored as the internal standard.

4.7. Diene−PyrNO Reactions Catalyzed by Tetrakis-(acetonitrile)copper(I) Hexafluorophosphate. In a drybox, 37 mg (0.10 mmol) of tetrakis(acetonitrile)copper(I) hexafluorophosphate was dissolved in 1.0 mL of methanol. In a Schlenk tube, 21.6 mg (0.20 mmol) of 2-nitrosopyridine was dissolved in 10 mL of methanol. The catalyst solution was injected into the nitrosopyridine solution (200 μL, 10% loaded), followed by the addition of 100 μL of 1,3-pentadiene (3 times excess, 75% pure, 2:1 E/Z) immediately to prevent any side reaction. The solution was left for 15 min, and then the solvent was evaporated to form a brown sticky mixture. One or two drops of acetone were added to the mixture to dissolve the solid, followed by the addition of 1.5 mL of 7:3 hexane:diethyl ether to precipitate side products. The isomeric product mixture was isolated after passing the supernatant solution through a silica plug and rotary evaporating the solvent. The ratio of the two products was determined by NMR integration.

4.8. Diene−PyrNO Reactions Catalyzed by (Diimine)$_2$copper(I) Hexafluorophosphate. In a drybox, 37 mg (0.10 mmol) of tetrakis(acetonitrile)copper(I) hexafluorophosphate was dissolved in 1.0 mL of methanol. In a different vial, imines were formed by adding 2 equiv (0.20 mmol) of the selected aldehyde (0.20 mmol), the selected amines (0.20 mmol), and methanol to make a 1.0 mL total solution volume. A red brown solution was formed upon mixing the imine and the copper solutions. The catalyst solution was left overnight to reach equilibrium. If dark brown crystals formed, more CH_3OH was added to dissolve the crystals then the solution was left overnight again. In a Schlenk tube, 22 mg (0.20 mmol) of 2-nitrosopyridine was dissolved in 10 mL of methanol. The catalyst solution was injected into the nitrosopyridine solution (1% loaded), followed by the addition of 100 μL of 1,3-pentadiene (3-fold excess, 75% pure, 2:1 E/Z) immediately to prevent any side reaction. The solution was left for 15 min, and then the solvent was evaporated to form a brown sticky mixture. One or two drops of acetone were added to the mixture to dissolve the solid, followed by the addition of 1.5 mL of 7:3 hexane:diethyl ether to precipitate side products. The isomeric product mixture was isolated after passing the supernatant solution through a silica plug and rotary evaporating the solvent. The ratio of the two products was determined by NMR integration. A list of *prox*/*dist* regioselectivities from the 1,3-pentadiene/PyrNO reactions catalyzed by various L_2Cu complexes is provided in the Supporting Information.

5. COMPUTATIONAL METHODS

All geometry optimizations and frequency calculations were performed with the M06 functional and a mixed basis set of SDD for Cu and 6-31G(d) for other atoms. The PCM solvation model was used in the geometry optimizations, and methanol was used as solvent. Single-point energies were calculated with M06 and a mixed basis set of SDD for Cu and 6-311+G(d,p) for other atoms. The PCM solvation model (methanol solvent) was also used in single-point energy calculations. All calculations were performed with Gaussian 09. All reported Gibbs free energies include zero-point vibrational energies and thermal corrections at 298 K. Energies in solution were converted to the standard state (1 mol/L). We also tested the B3LYP functional, calculations in gas phase, and single-point energies with a different basis set. The benchmark results on activation barriers of the reaction of 2-nitrosopyridine and (*E*)-1,3-pentadiene are summarized in Table 1. The M06/6-311+G(d,p)-SDD(PCM)//M06/6-31G(d)-SDD-(PCM) gives excellent agreement with the experimental regioselectivity for the benchmark calculations.

■ ASSOCIATED CONTENT

Ⓢ Supporting Information

2D, NOE data for isomeric adducts; X-ray data collection table and *x*,*y*,*z* coordinates for **28**; table of L_2Cu-catalysts and *prox*/*dist* adduct regioselectivity; complete reference of Gaussian 09, and optimized geometries (*x*,*y*,*z* coordinates) and energies of all computed species. This material is available free of charge via the Internet at http://pubs.acs.org.

■ AUTHOR INFORMATION

Corresponding Author

*E-mail: knicholas@ou.edu.

Notes

The authors declare no competing financial interest.

■ ACKNOWLEDGMENTS

We are grateful to Drs. Susan Nimmo, Stephen Foster, and Douglas Powell (O.U. Analytical Services Center) for their assistance with NMR, MS, and X-ray crystallographic analyses, respectively. We also thank the National Science Foundation for financial support through CHE-0911158 (K.M.N.) and CHE-1059084 (K.N.H.). Calculations were performed on the Hoffman2 cluster at UCLA and the Extreme Science and Engineering Discovery Environment (XSEDE), which is supported by the NSF.

■ REFERENCES

(1) (a) Kirby, G. W.; Nazeer, M. *J. Chem. Soc., Perkin Trans. 1* **1993**, *13*, 1397−402. (b) Freer, A. A.; Islam, M. A.; Kirby, G. W.; Mahajan, M. P. *J. Chem. Soc., Perkin Trans. 1* **1991**, *5*, 1001−1007. (c) Corrie, J. E. T.; Kirby, G. W.; Mackinnon, J. W. M. *J. Chem. Soc., Perkin Trans. 1*

1985, *4*, 883−886. (d) Kirby, G. W.; Bentley, K. W.; Horsewood, P.; Singh, S. *J. Chem. Soc., Perkin Trans. 1* **1979**, *12*, 3064−3066.
(2) Li, J.; Lang, F.; Ganem, B. *J. Org. Chem.* **1998**, *63*, 3403.
(3) Aoyagi, S.; Tanaka, R.; Naruse, M.; Kibayashi, C. *J. Org. Chem.* **1998**, *63*, 8397.
(4) Jana, C. K.; Studer, A. *Chem.—Eur. J.* **2008**, *14*, 6326.
(5) Li, F.; Brogan, J. B.; Gage, J. L.; Zhang, D.; Miller, M. J. *J. Org. Chem.* **2004**, *69*, 4538.
(6) Yamamoto, H.; Kawasaki, M. *Bull. Chem. Soc. Jpn.* **2007**, *80*, 595.
(7) Bodnar, B. S.; Miller, M. J. *Angew. Chem., Int. Ed.* **2011**, *50*, 5630.
(8) Iwasa, S.; Ahmad, F.; Nishiyama, H. *Mini-Rev. Org. Chem.* **2005**, *2*, 157.
(9) Krchňák, V.; Moellmann, U.; Dahse, H.-M.; Miller, M. J. J. *Comb. Chem.* **2008**, *10*, 104.
(10) Lin, W.; Gupta, A.; Kim, K. H.; Mendel, D.; Miller, M. J. *Org. Lett.* **2009**, *11*, 449.
(11) Li, F.; Yang, B.; Miller, M. J.; Zajicek, J.; Noll, B. C.; Möllmann, U.; Dahse, H.-M.; Miller, P. A. *Org. Lett.* **2007**, *9*, 2923.
(12) Labaziewicz, H. L.; Karl, R.; Kejonen, T. H. *Heterocycles* **1989**, *29*, 2327.
(13) Yang, B.; Miller, P. A.; Möllmann, U.; Miller, M. J. *Org. Lett.* **2009**, *11*, 2828.
(14) Yamamoto, Y.; Yamamoto, H. *J. Am. Chem. Soc.* **2004**, *126*, 4128.
(15) Yamamoto, Y.; Yamamoto, H. *Angew. Chem., Int. Ed.* **2005**, *44*, 7082.
(16) Chow, C. P.; Shea, K. J. *J. Am. Chem. Soc.* **2005**, *127*, 3678.
(17) Momiyama, N.; Yamamoto, H. *J. Am. Chem. Soc.* **2004**, *126*, 5360.
(18) Flower, K. R.; Lightfoot, A. P.; Wan, H.; Whiting, A. *J. Chem. Soc., Perkin Trans. 1* **2002**, *18*, 2058.
(19) Leach, A. G.; Houk, K. N. *J. Org. Chem.* **2001**, *66*, 5192.
(20) McCarrick, M. A.; Wu, Y. D.; Houk, K. N. *J. Org. Chem.* **1993**, *58*, 3330.
(21) Leach, A. G.; Houk, K. N. *Chem. Commun.* **2002**, *0*, 1243.
(22) Jana, C. K.; Grimme, S.; Studer, A. *Chem.—Eur. J.* **2009**, *15*, 9078.
(23) Jana, C. K.; Studer, A. *Angew. Chem., Int. Ed.* **2007**, *46*, 6542.
(24) Bollans, L.; Bacsa, J.; O'Farrell, D. A.; Waterson, S.; Stachulski, A. V. *Tetrahedron Lett.* **2010**, *51*, 2160.
(25) Calvet, G.; Blanchard, N.; Kouklovsky, C. *Synthesis* **2005**, *2005*, 3346.
(26) Miller, C. A.; Batey, R. A. *Org. Lett.* **2004**, *6*, 699.
(27) Yang, B.; Lin, W.; Krchnak, V.; Miller, M. J. *Tetrahedron Lett.* **2009**, *50*, 5879.
(28) Resmini, M.; Meekel, A. A. P.; Pandit, U. K. *Pure Appl. Chem.* **1996**, *68*, 2025.
(29) Meekel, A. A. P.; Resmini, M.; Pandit, U. K. *J. Chem. Soc., Chem. Commun.* **1995**, 571.
(30) Reymond, S. B.; Cossy, J. *Chem. Rev.* **2008**, *108*, 5359.
(31) Fringuelli, F.; Piermatti, O.; Pizzo, F.; Vaccaro, L. *Eur. J. Org. Chem.* **2001**, 439.
(32) Markó, I. E.; Evans, G. R.; Seres, P.; Chellé, I.; Janousek, Z. *Pure Appl. Chem.* **1996**, *68*, 113.
(33) Matsumoto, M.; Estes, D.; Nicholas, K. M. *Eur. J. Inorg. Chem.* **2010**, 1847.
(34) Miller, B. L., Ed. *Dynamic Combinatorial Chemistry In Drug Discovery, Bioorganic Chemistry and Materials Science*; Wiley: Hoboken, NJ, 2009.
(35) Ladame, S. *Org. Biomol. Chem.* **2008**, *6*, 219.
(36) Corbett, P. T.; Leclaire, J.; Vial, L.; West, K. R.; Wietor, J. L.; Sanders, J. K. M.; Otto, S. *Chem. Rev.* **2006**, *106*, 3652.
(37) Lehn, J.-M. *Chem. Soc. Rev.* **2007**, *36*, 151.
(38) Gasparini, G.; Molin, M. D.; Prins, L. J. *Eur. J. Org. Chem.* **2010**, 2429.
(39) Breuil, P.-A. R.; Reek, J. N. H. Dynamic Combinatorial Chemistry for Catalytic Applications. In *Dynamic Combinatorial Chemistry*; Reek, J. N. H., Otto, S., Eds.; Wiley-VCH: Weinheim, Germany, 2010.
(40) Kannappan, R.; Matsumoto, M.; Hallren, J.; Nicholas, K. M. *J. Mol. Catal. A: Chem.* **2011**, *339*, 72.
(41) Kannappan, R.; Nicholas, K. M. *ACS Comb. Sci.* **2013**, *15*, 90.
(42) (a) Zhao, Y.; Truhlar, D. G. *Theor. Chem. Acc.* **2008**, *120*, 215. (b) Zhao, Y.; Truhlar, D. G. *Acc. Chem. Res.* **2008**, *41*, 157.
(43) The default PCM (IEFPCM) solvation model in Gaussian 09 D.01 was implemented: (a) Tomasi, J.; Mennucci, B.; Cammi, R. *Chem. Rev.* **2005**, *105*, 2999−3093. (b) Scalmani, G.; Frisch, M. J. *J. Chem. Phys.* **2010**, *132*, 114110.
(44) Lam, Y.-H.; Cheong, P. H.-Y.; Blasco Mata, J. M.; Stanway, S. J.; Gouverneur, V.; Houk, K. N. *J. Am. Chem. Soc.* **2009**, *131*, 1947.
(45) Pieniazek, S. N.; Clemente, F. R.; Houk, K. N. *Angew. Chem., Int. Ed.* **2008**, *47*, 7746.
(46) Siegert, U.; Hahn, H.; Lang, H. *Inorg. Chim. Acta* **2010**, *363*, 944.
(47) Nitschke, J. R. *Acc. Chem. Res.* **2007**, *40*, 103.
(48) Riesgo, E.; Hu, Y.-Z.; Bouvier, F.; Thummel, R. P. *Inorg. Chem.* **2001**, *40*, 2541.
(49) Birney, D. M.; Houk, K. N. *J. Am. Chem. Soc.* **1990**, *112*, 4127.
(50) Taylor, E. C.; Tseng, C. P.; Rampal, J. B. *J. Org. Chem.* **1982**, *47*, 552.
(51) Lishchynskyi, A.; Muñiz, K. *Chem.—Eur. J.* **2012**, *18*, 2212.